

# The role of nitrogen doping in ALD Ta<sub>2</sub>O<sub>5</sub> and its influence on multilevel cell switching in RRAM

N. Sedghi<sup>1, a)</sup>, H. Li<sup>2</sup>, I. F. Brunell<sup>3</sup>, K. Dawson<sup>3</sup>, R. J. Potter<sup>3</sup>, Y. Guo<sup>4</sup>, J. T. Gibbon<sup>5</sup>, V. R. Dhanak<sup>5</sup>, W. D. Zhang<sup>6</sup>, J. F. Zhang<sup>6</sup>, J. Robertson<sup>2</sup>, S. Hall<sup>1</sup>, and P. R. Chalker<sup>3</sup>

<sup>1</sup>*Department of Electrical Engineering and electronics, University of Liverpool, Liverpool, L69 3GJ, United Kingdom*

<sup>2</sup>*Department of Engineering, University of Cambridge, Cambridge, CB2 1TN, United Kingdom*

<sup>3</sup>*School of Engineering, University of Liverpool, Liverpool, L69 3GH, United Kingdom*

<sup>4</sup>*College of Engineering, Swansea University, Swansea SA1 8EN, United Kingdom*

<sup>5</sup>*Department of Physics, University of Liverpool, Liverpool, L69 7ZE, United Kingdom*

<sup>6</sup>*Department of Electronics and Electrical Engineering, Liverpool John Moores University, Liverpool, L3 3AF, United Kingdom*

The role of nitrogen doping on the stability and memory window of resistive state switching in N-doped Ta<sub>2</sub>O<sub>5</sub> deposited by atomic layer deposition is elucidated. Nitrogen incorporation increases the stability of resistive memory states which is attributed to neutralization of electronic defect levels associated with oxygen vacancies. The density functional simulation with screened exchange hybrid functional approximation finds that the incorporation of nitrogen dopant atoms in the oxide network removes the O vacancy midgap defect states, thus nullifying excess defects and eliminating alternative conductive paths. By effectively reducing the density of vacancy-induced defect states through N doping, 3-bit multilevel cell switching is demonstrated, consisting of eight distinctive resistive memory states achieved by either controlling the set current compliance or the maximum voltage during reset. Nitrogen doping has a threefold effect; widening the switching memory window to accommodate more intermediate states, improving the stability of states, and providing gradual reset for multi-level cell switching during reset. The N-doped Ta<sub>2</sub>O<sub>5</sub> devices have relatively small set and reset voltages (< 1 V) with reduced variability due to doping.

Resistive-switching random access memory (RRAM) is the focus of development as a substitute for existing non-volatile memory (NVM) devices. In metal oxide based RRAM devices, switching between low resistive and high resistive states (LRS and HRS, respectively) occurs by field-assisted diffusion of defects such as oxygen vacancies (O<sub>vac</sub>), to form a conductive “filament” (CF)<sup>1</sup>. By applying appropriate voltages across the oxide, the CF can be formed, ruptured, and restored to switch between the “on” and “off” memory states. It is crucial to engineer the oxygen vacancy profile in the oxide film to achieve stable memory states and a large switching memory window for immunity to noise. Extending this requirement further leads

---

<sup>a)</sup> Corresponding author electronic mail: nsed@liverpool.ac.uk.

to the prevention of multiple potential CFs with different LRS resistances, which is the main cause of the variability in the multilevel cell (MLC) switching states<sup>2</sup>. The MLC enables multi-bit storage capacity and potentially increases the storage capacity for ultra-high density memory applications. It has been reported that the variability of resistance associated with a CF depends on the conductive filament size and also the oxygen vacancy concentration<sup>3</sup>. The multilevel switching is commonly achieved by adjusting the LRS current by changing the compliance during the set cycle<sup>2-5</sup>. Less common is to change the HRS current by changing the maximum voltage during the reset<sup>5, 6</sup>. In both methods, achieving more than 2-bit storage (4 distinctive states) is challenging due to the variability of states and small switching memory window. 3-bit MLC switching has only been reported on LRS current varied by the set current compliance method<sup>2, 4</sup>. However, the MLC performance reported was on small area (250 nm diameter) devices which allow small set currents down to 10  $\mu$ A and enhanced stability of states. Here, we have combined the two MLC switching methods using N-doped atomic layer deposited (ALD) Ta<sub>2</sub>O<sub>5</sub> based RRAM devices, which facilitates the achievement 3-bit MLC by varying the low resistance states in the upper half of the memory window by set current compliance and high resistance states in the lower part by maximum voltage during reset. The role of N doping is controlling the oxygen density in the film, firstly to widen the memory window to accommodate more intermediate states, secondly, to improve the stability of states, and thirdly, providing gradual reset which is essential for MLC switching of HRS resistance.

The selection of appropriate switching layer material is central to the RRAM operation<sup>7</sup> and tantalum oxide is of particular interest because of high endurance of switching cycles<sup>8</sup>. The purpose of N doping is to reduce electronic defect states associated with the O<sub>vac</sub><sup>9</sup> and enabling CFs to be formed with more stable and discrete resistances suitable for MLC. The state stability necessary for MLC is believed to be due to the elimination of excess conducting paths in the oxide by passivation of oxygen vacancies by nitrogen atoms<sup>2</sup>.

Metal-insulator-metal (MIM) structures were fabricated on both Corning glass and silicon wafer substrates. A plan view and the bright field transmission electron microscopy (BF-TEM) micrograph of the MIM structure are shown in Fig. 1. The bottom electrode is 50 nm Pt, with 10 nm Cr adhesion layer, deposited by dc magnetron sputtering. The oxide layer, Ta<sub>2</sub>O<sub>5</sub> or N-doped Ta<sub>2</sub>O<sub>5</sub>, was deposited by conventional ALD, using the precursor Ta(OC<sub>2</sub>H<sub>5</sub>)<sub>5</sub> and H<sub>2</sub>O as an oxidant. N doping was achieved by substituting a proportion of the water cycles with aqueous NH<sub>4</sub>OH solution. The level of N incorporated in the film was estimated to be 9 % by X-ray photoelectron spectroscopy (XPS). The top electrode of 30 nm Ti, with 60 nm of Pt capping layer, was deposited by rf sputtering. Conventional photolithography and lift off were used to define the top and bottom contacts and device active area of 512 overlapping and 512 cross-line square devices with dimensions of 2 to 150  $\mu$ m. The dc set-reset cycles were performed by either HP 4155A or Agilent B1500A Semiconductor Parameter Analyzers.

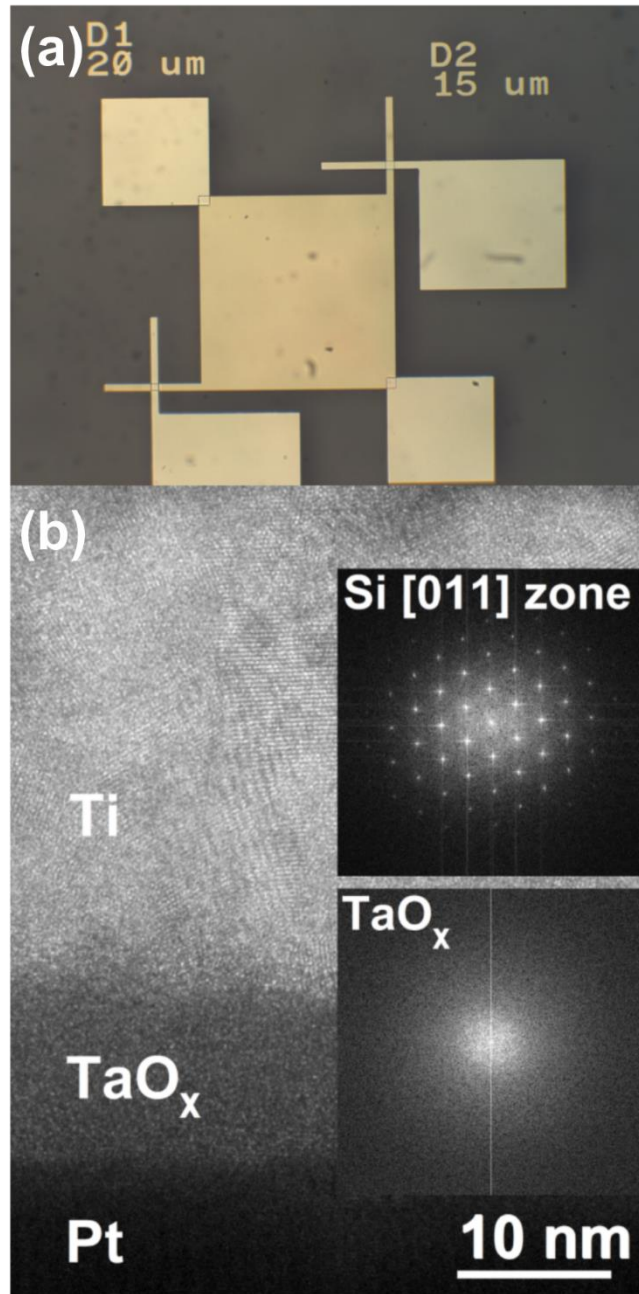


FIG. 1. (a) Plan view and (b) BF-TEM image of device cross section.

The switching characteristics are independent of device area ( $4\text{-}22500\text{ }\mu\text{m}^2$ ), which is consistent with previous reports<sup>8</sup> and indicates the presence of only one dominant conductive filament at a time in one device. Figure 2 (a) shows switching characteristics of the devices made of undoped and N-doped  $\text{Ta}_2\text{O}_5$  with 8 % doping cycles at a set current compliance of 1 mA. A significant increase in memory window, from 15 to 150 at  $-0.1\text{ V}$ , due to reduction in HRS current is apparent in the N-doped device, which is attributed to a more resistive ruptured region of conductive filament. There is a slight increase in LRS current in the N-doped sample which indicates the increase in conductance of the filament in that device. Previously, a

reduction of both HRS and LRS currents in an N-doped device has been reported, which was attributed to the elimination of excess conducting paths resulting in a narrower filament<sup>2</sup>. The LRS current is governed by metallic conduction which depends on the conductivity and average radius of the filament. Furthermore, a reduction in  $O_{vac}$ , in this case by N doping, increases the conductivity of the filament by eliminating the excess conductive paths which results in a denser localized conductive filament<sup>4</sup> with smaller inter-atomic distance between O vacancies. Reduction of  $O_{vac}$  also reduces the average radius of the filament, resulting in reduction in LRS current. Whether the LRS current has an increase or decrease with N doping, depends on various factors including the amount of doping and set current compliance. The HRS current, however, is controlled by the ruptured region in the conductive filament. The decreased HRS current in the doped device can be attributed to a longer ruptured region of the filament and longer hopping distance due to a lower concentration of O vacancies.

The effect of set current compliance and maximum voltage during reset ( $V_{max}$ ) on an N-doped device is shown in Fig. 2 (b) and (c), respectively. Varying the former, changes the LRS current and varying the latter changes the HRS current, both resulting in intermediate states within the upper and lower parts of the memory window, respectively, resulting in MLC switching behavior. The increase in LRS current with increase in set current compliance is related to larger radius of the conductive filament and also the higher concentration of O vacancies within the filament<sup>3</sup>. The reduction in HRS current with  $V_{max}$  is due to a larger emigration rate of oxygen vacancies from conductive filament, resulting in a wider ruptured region.

For MLC switching with a large number of intermediate states (3-bit or more), the device not only requires a large memory window to accommodate the states, but also the states need to have small variability to prevent intermixing. It has been shown in the literature<sup>3, 4</sup> and is shown in this work that atomic doping can improve both requirements. Evolution of a conductive filament and its rupture and restoration have been studied by various analytical and numerical models<sup>10-14</sup> which can shed light on the device switching characteristics and the stability of states. The cumulative distribution function (CDF) of the resistance at various states read at voltage of  $-0.1$  V is shown in Fig. 3 with good separation between 8 states. This provides a 3-bit MLC, consisting of four LRS and four HRS intermediate states.

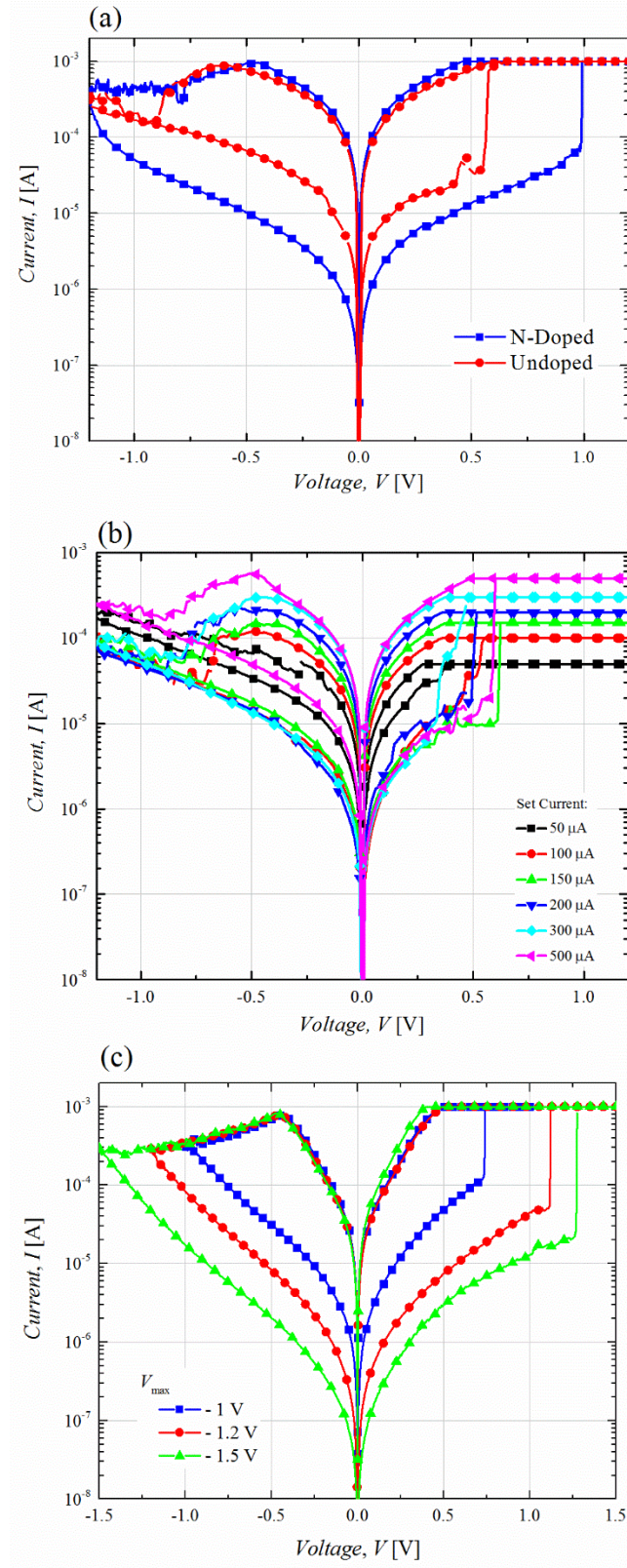


FIG. 2. (a) The switching characteristics of the N-doped and undoped RRAM devices at set current compliance of 1 mA. Variation of LRS current with set current compliance (b) and HRS with  $V_{\max}$  (c).

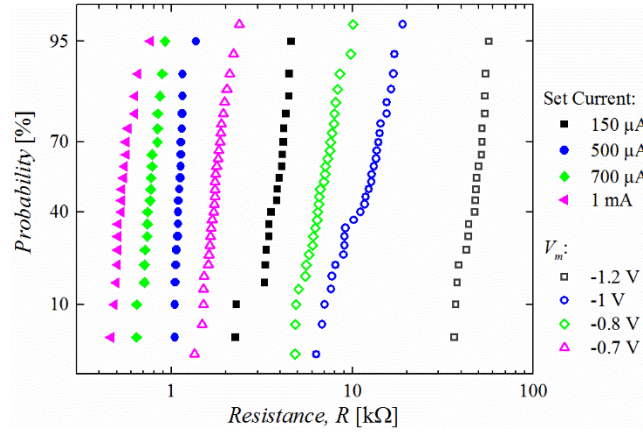


FIG. 3. The cumulative distribution function (CDF) of the resistance at various states read at voltage of  $-0.1$  V.

We have previously reported the properties of  $O_{vac}$  in the  $\lambda$  phase of  $Ta_2O_5$  crystal<sup>15</sup> and in the amorphous  $Ta_2O_5$  network<sup>16</sup> through sX density functional simulations. It is found that the 2-fold  $O_{vac}$  in both networks has a small formation energy, low diffusion barrier, and deep defect states below the conduction band, believed to be strongly related to the resistive switching behavior in the RRAM devices. Here we have applied the sX hybrid functional density functional simulation to calculate the effect of N doping in the amorphous  $Ta_2O_5$  network. The simulation settings are the same as in our previous work<sup>16</sup>. The atomic structure and density of states (DOS) of the amorphous  $Ta_2O_5$  network with a 2-fold  $O_{vac}$  is shown in Fig. 4 (a, b). The  $O_{vac}$  gives rise to a deep defect state in the mid bandgap region, with the defect orbital localized on one nearby Ta atom. The effect of N doping has been studied by substituting two O atoms with N atoms near the  $O_{vac}$  site, as shown in Fig. 4 (c). The original  $O_{vac}$  defect state in the bandgap is removed as a result of N doping<sup>9</sup>, leaving some N bonding states near the valence band of  $Ta_2O_5$ .

We now consider the mechanism of such a doping effect. The original  $O_{vac}$  introduces two excess electrons localized on the nearby Ta atom. During the doping process, each N atom substitutes one O atom in the network, and creates a valence band hole. The two excess electrons from  $O_{vac}$  transfer to two nearby N atoms to fill their valence states and form a closed shell electronic configuration. Locally, the  $O_{vac}$  becomes a  $V^{2+}$  center, involving a certain lattice distortion, and pushes the original defect state up into conduction band<sup>9</sup>. The energy gain of this process comes from the two electrons falling from mid gap states into valence band holes, which compensates the energy required for local distortion. In this way, the 2-fold  $O_{vac}$  in the amorphous  $Ta_2O_5$  network is nullified or cancelled by the presence of two N atoms. The neutralization of the defect states associated with the  $O_{vac}$  eliminates the excess conductive paths<sup>4</sup> and reduces the numbers or densities of potential filaments. This effect has been observed in sputtered  $TaO_x$  films by controlling the oxygen partial pressure during sputtering<sup>3</sup>. It was



concluded that the variability of the conductive filament resistance depends on both the filament diameter and the oxygen vacancy density in the filament. The model presented here shows that the effect of adding nitrogen to the ALD tantalum oxide can help to improve these factors and that multilevel switching is achievable in the 8 % doped film. It reduces the variability in LRS current by preventing the set operation of the device through a different conductive path. It also makes the filament denser which increases the LRS current due to larger conductance and decreases the HRS current due to a larger gap in the ruptured filament at critical filament region.

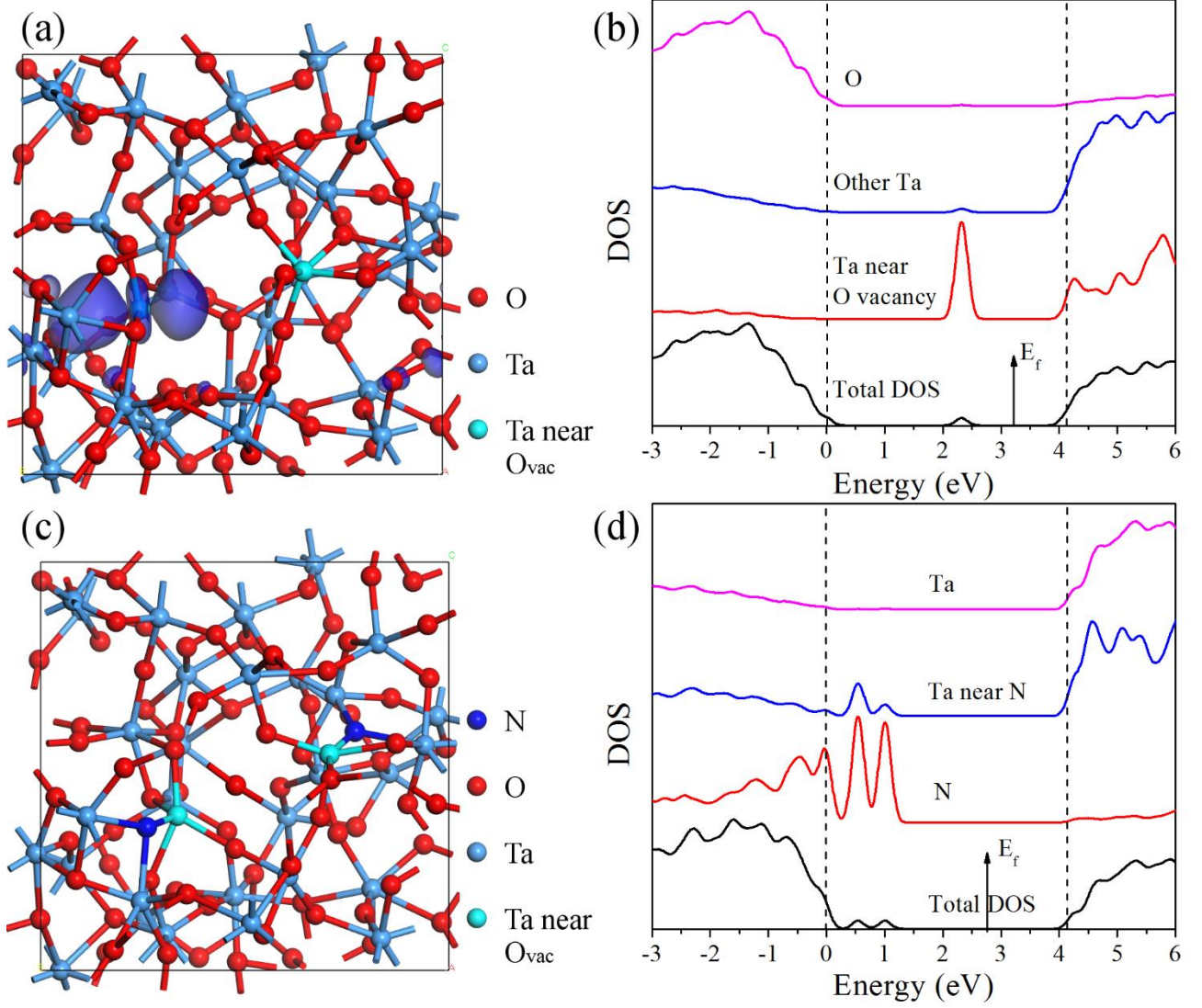


FIG. 4. (a) The atomic model and (b) the density of states of undoped amorphous  $\text{Ta}_2\text{O}_5$  structure with an O vacancy. The blue isosurface shows defect orbital in mid bandgap. (c) The atomic model and (d) the density of states of amorphous  $\text{Ta}_2\text{O}_5$  structure with two N atoms substituting two O atoms near the O vacancy site. The red, light blue, cyan, and dark blue balls denote O, Ta, Ta near O vacancy, and N atoms, respectively.

In conclusion, RRAM devices were fabricated by ALD Ta<sub>2</sub>O<sub>5</sub> doped with nitrogen. The dc sweep set-reset measurements show that passivation of O<sub>vac</sub> increases the switching memory window and states stability. The stability of states and the separation of states at various set currents enables the device for MLC switching applications. The devices have set and reset voltages of less than 1 V and their variability is improved by doping. Density functional simulation of the atomic structures and calculation of density of states using sX hybrid functional correction show that N dopants substitute O atoms near the O<sub>vac</sub>, resulting in nullifying the associated electronic defect states in the mid bandgap of the oxide, and thus eliminates alternative conductive paths.

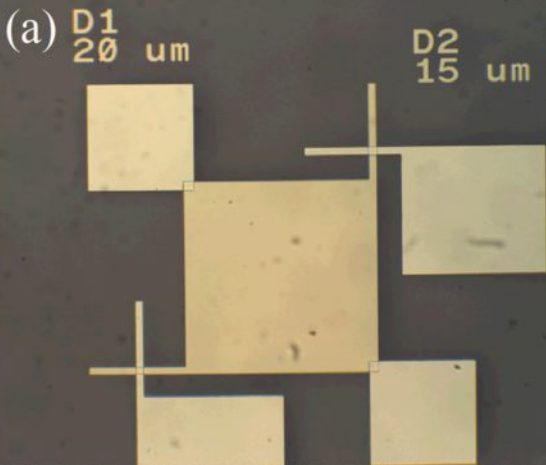
The work has been funded by the Engineering and Physical Sciences Research Council (EPSRC) UK, project numbers EP/M00662X/1, EP/M009297/1 and EP/M006727/1.

- <sup>1</sup>H. Akinaga and H. Shima, P. IEEE **98**, 2237 (2010).
- <sup>2</sup>S. H. Misha, N. Tamanna, J. Woo, S. Lee, J. Song, J. Park, S. Lim, J. Park, and H. Hwang, ECS Solid State Lett. **4**, P25 (2015).
- <sup>3</sup>A. Prakash, D. Deleruyelle, J. Song, M. Bocquet, and H. Hwang, App. Phys. Lett. **106**, 233104-1 (2015).
- <sup>4</sup>A. Prakash, J. Park, J. Song, J. Woo, E. J. Cha, and H. Hwang, IEEE Electron Device L. **36**, 32 (2015).
- <sup>5</sup>M. C. Wu, W. Y. Jang, C. H. Lin, and T. Y. Tseng, Semicond. Sci. Technol. **27**, 065010 (2012).
- <sup>6</sup>S. Yu, Yi Wu, and H.-S. P. Wong, Appl. Phys. Lett. **98**, 103514-1 (2011).
- <sup>7</sup>Y. Guo and J. Robertson, Appl. Phys. Lett. **105**, 223516-1 (2014).
- <sup>8</sup>M. J. Lee, C. B. Lee, D. Lee, S. R. Lee, M. Chang, J. H. Hur, Y. B. Kim, C. J. Kim, D. H. Seo, S. Seo, U. I. Chung, I. K. Yoo, and K. Kim, Nat. Mater. **10**, 625 (2011).
- <sup>9</sup>K. Xiong, J. Robertson, and S. J. Clark, J. Appl. Phys. **99**, 044105-1 (2006); H. Li, Y. Guo, and J. Robertson, Appl. Phys. Lett. **104**, 192904-1 (2014).
- <sup>10</sup>D. Ielmini, IEEE T. Electron Dev. **58**, 4309 (2011).
- <sup>11</sup>D. Ielmini, Semicond. Sci. Technol. **31**, 063002-1 (2016).
- <sup>12</sup>S. Ambrogio, S. Balatti, and V. McCaffrey, IEDM Tech. Dig., 363 (2014).
- <sup>13</sup>P. Sun, S. Liu, L. Li, and M. Liu, J. Semicond. **35**, 104007-1 (2014).
- <sup>14</sup>S. Kim, S. J. Kim, K. M. Kim, S. R. Lee, M. Chang, E. Cho, Y. B. Kim, C. J. Kim, U. I. Chung, and I. K. Yoo, Sci. Rep. **3:1680**, 1 (2013).



<sup>15</sup>Y. Guo and J. Robertson, Appl. Phys. Lett. **104**, 112906-1 (2014).

<sup>16</sup>Y. Guo and J. Robertson, Microelectron. Eng. **147**, 254 (2015).



(b)

**Ti**

**TaO<sub>x</sub>**

**Pt**

**Si [011] zone**

**TaO<sub>x</sub>**

**10 nm**

